



1 **Projected future changes in cryosphere and hydrology of a**  
2 **mountainous catchment in the Upper Heihe River, China**

3

4 Zehua Chang <sup>1</sup>, Hongkai Gao <sup>1\*</sup>, Leilei Yong <sup>1</sup>, Kang Wang <sup>1</sup>, Rensheng Chen <sup>2</sup>,  
5 Chuntan Han <sup>2</sup>, Otgonbayar Demberel <sup>3</sup>, Batsuren Dorjsuren <sup>4</sup>, Shugui Hou <sup>5</sup>, Zheng  
6 Duan <sup>6</sup>

7 <sup>1</sup> Key Laboratory of Geographic Information Science (Ministry of Education of  
8 China), School of Geographical Sciences, East China Normal University, Shanghai,  
9 China

10 <sup>2</sup> Qilian Alpine Ecology and Hydrology Research Station, Key Laboratory of  
11 Ecohydrology of Inland River Basin, Northwest Institute of Eco-Environment and  
12 Resources, Chinese Academy of Sciences, Lanzhou 730000, China

13 <sup>3</sup> Department of Geography and Geology Khovd branch of National University of  
14 Mongolia, Erkh choolonii street, Khovd, Mongolia

15 <sup>4</sup> Department of Environment and Forest Engineering, National University of  
16 Mongolia, Ulaanbaatar 210646, Mongolia

17 <sup>5</sup> School of Oceanography (SOO), Shanghai Jiao Tong University (SJTU), Shanghai,  
18 China

19 <sup>6</sup> Department of Physical Geography and Ecosystem Science, Lund University,  
20 Sölvegatan 12, SE-223 62, Lund, Sweden

21 \*Correspondence: Hongkai Gao (hkgao@geo.ecnu.edu.cn)

22

23 **Abstract:** Climate warming exacerbates the degradation of the mountain cryosphere,  
24 including glacier retreat, reduction in snow cover area, and permafrost degradation.

25 These changes dramatically alter the local and downstream hydrological regime,  
26 posing significant threats to basin-scale water resource management and sustainable  
27 development. However, there is still a lack of systematic research that evaluates the  
28 variation of cryospheric elements in mountainous catchments and their impacts on



29 future hydrology and water resources. In this study, we developed an integrated  
30 cryospheric-hydrologic model, referred to as the FLEX-Cryo model. This model  
31 comprehensively considers glaciers, snow cover, frozen soil, and their dynamic  
32 impacts on hydrological processes in the mountainous Hulu catchment located in the  
33 Upper Heihe river of China. We utilized the state-of-the-art climate change projection  
34 data from the sixth phase of the Coupled Model Intercomparison Project (CMIP6) to  
35 simulate the future changes in the mountainous cryosphere and their impacts on  
36 hydrology. Our findings showed that the two glaciers in the Hulu catchment will  
37 completely melt out around the years 2045-2051. By the end of the 21st century, the  
38 annual maximum snow water equivalent is projected to decrease by 41.4% and  
39 46.0%, while the duration of snow cover will be reduced by approximately 45 and 70  
40 days. The freeze onset of seasonal frozen soil is expected to be delayed by 10 and 22  
41 days, while the thaw onset of permafrost is likely to advance by 19 and 32 days.  
42 Moreover, the maximum freeze depth of seasonal frozen soil is projected to decrease  
43 by 5.2 and 10.9 cm per decade, and the depth of the active layer will increase by 8.2  
44 and 15.5 cm per decade. Regarding hydrology, runoff exhibits a decreasing trend until  
45 the complete melt-out of glaciers, resulting in a total runoff decrease of 15.6% and  
46 18.1%. Subsequently, total runoff shows an increasing trend, primarily due to an  
47 increase in precipitation. Permafrost degradation causes the duration of low runoff in  
48 the early thawing season to decrease, and the discontinuous baseflow recession  
49 gradually transitions into linear recessions, leading to an increase in baseflow. Our  
50 results highlight the significant changes expected in the mountainous cryosphere and  
51 hydrology in the future. These findings enhance our understanding of cold-region  
52 hydrological processes and have the potential to assist local and downstream water



53 resource management in addressing the challenges posed by climate change.

54 **Keywords:** Glacier, Snow cover, Seasonal frozen soil, Permafrost, Runoff, Model  
55 prediction

56

## 57 1. Introduction

58 “How will cold region runoff and groundwater change in a warmer climate?”  
59 was identified by the International Association of Hydrological Sciences (IAHS) as  
60 one of the 23 unsolved scientific problems (Blöschl et al., 2019). The mountain  
61 cryosphere, which includes glaciers, snow cover, and frozen soil in high-altitude  
62 regions, has a significant impact on water resources (Adler et al., 2019; Arendt et al.,  
63 2020; Rasul et al., 2020; Zhang et al., 2022). Mountain cryosphere is considered a  
64 crucial "water tower" and a climate change indicator due to its sensitivity to climate  
65 change (Tang et al., 2023). However, the cryosphere is rapidly retreating in many  
66 parts of the world, including glacier retreat, expansion of glacier lakes, northward  
67 movement of the permafrost southern limit, and shrinking snow cover area (Moreno  
68 et al., 2022; S. Wang et al., 2022; Ding et al., 2019; Wang et al., 2023). These changes  
69 have disrupted the water tower region and pose significant challenges to sustainable  
70 water resources management (Ragettli et al., 2016; Yao et al., 2022).

71 The degradation of the mountain cryosphere varies from region to region  
72 (Andrianaki et al., 2019; Wang et al., 2019). Lower altitudes experience a decreasing  
73 trend in snow cover days, snow depth, snow water equivalent, and snowmelt due to  
74 climate warming, while higher altitudes present a more complex picture (Connon et  
75 al., 2021; Nury et al., 2022; Yang et al., 2022). Global continental glacier mass  
76 balance from 2006 to 2015 was approximately  $-123 \pm 24$  GT yr<sup>-1</sup>, with significant



77 losses observed in the Southern Andes, Caucasus Mountains, and Central Europe,  
78 while the Karakoram and Pamir regions exhibited lesser loss (Intergovernmental  
79 Panel on Climate Change (IPCC), 2022; Van Der Geest and Van Den Berg, 2021).  
80 Future projections suggest a 40% decrease in global permafrost by the end of the  
81 century, potentially transitioning into seasonal frozen soil (Chadburn et al., 2017). The  
82 mountain cryosphere serves as a significant freshwater reservoir, impacting water  
83 resources and the hydrological cycle (Ding et al., 2020).

84 In a warming climate, glacier runoff exhibits a "tipping point" characterized by  
85 an initial increase followed by a subsequent decline (Rosier et al., 2021; Zhang et al.,  
86 2012). While small glaciers have already experienced this tipping point, its  
87 occurrence in large glaciers remains uncertain (Brovkin et al., 2021; Huss and Hock,  
88 2018). Permafrost degradation leads to an increase in active layer thickness, resulting  
89 in the melting of subsurface ice and an augmentation of soil water storage capacity  
90 (Abdelhamed et al., 2022). Additionally, the degradation of the cryosphere  
91 significantly impacts the atmosphere, biosphere, surface energy balance, ecological  
92 water use, and ecosystems (Gilg et al., 2012; Miner et al., 2022; Pothula and Adams,  
93 2022). Understanding the complex interactions between cryosphere degradation and  
94 ecosystems is crucial, but quantitatively observing the degradation process in high-  
95 altitude regions is challenging. Hydrological models provide an effective approach to  
96 analyze degradation patterns and assess the impact on future water resources (Han and  
97 Menzel, 2022).

98 Glacio-hydrology is influenced by both glacier melt and glacier dynamics.  
99 Glacier melting models can be categorized into three types: energy balance,  
100 temperature index, and hybrid models (He et al., 2021; Gao et al., 2021; Negi et al.,



101 2022; Zekollari et al., 2022). While energy balance models analyze glacier  
102 accumulation and melt processes based on solid physical mechanisms, they require  
103 extensive forcing data that may not be readily available in mountainous regions (Huss  
104 et al., 2010). On the other hand, temperature index models are simpler and more  
105 effective, requiring fewer parameters (including degree-day factor and threshold  
106 temperature) and forcing data (temperature and precipitation) (Bolibar et al., 2022;  
107 Vincent and Thibert, 2023). It performs well at both daily and monthly scales.  
108 Glaciers are moving slowly, due to the combined effects of gravity and high viscosity  
109 of ice. Due to climate change, ice becomes thinner, and glacier loses its mass balance,  
110 which will cause the glacier morphology evolve to a new balance status. Glacier  
111 dynamic models, with full-Stokes approach as the most complete form, and many  
112 other simplifications, such as the shallow-ice approximation, and the shallow-shelf  
113 approximation etc, are still computationally expensive, hindering their implications in  
114 large scale studies. Three conceptual models are commonly used for glacier evolution:  
115 volume-area scaling (V-A) method, accumulation area ratio (AAR) method, and  $\Delta h$ -  
116 parameterization (Michel et al., 2022; Wiersma et al., 2022). The first two approaches  
117 do not consider the detailed changes in different elevation bands, while the  $\Delta h$ -  
118 parameterization approaches only require glacier mass balance as forcing data to  
119 analyze changes in ice thickness at different elevation bands based on the relationship  
120 between glacier mass balance and glacier area (Huss et al., 2010). The temperature  
121 index method coupled with the  $\Delta h$ -parameterization approach serve as effective  
122 module to simulate glacier evolution and its impacts on hydrology.

123 Permafrost hydrology models can be classified into one-dimensional models and  
124 distributed watershed models (Elshamy et al., 2020). One-dimensional hydrological



125 models, such as the Stefan equation, the temperature at the top of permafrost (TTOP)  
126 model, CoupModel, and SHAW model, are effective in simulating freeze depth,  
127 hydrothermal transport, and carbon or nitrogen transport, but they are unable to  
128 capture the broader impact of permafrost on hydrology at catchment scale (Kaplan  
129 Pastřířková et al., 2023; Li et al., 2022; Liu et al., 2023). On the other hand,  
130 distributed watershed models, such as the Cold Regions Hydrological Model  
131 (CRHM), Hydrogeosphere (HGS), and Distributed water-heat coupled model  
132 (DWHC), consider the spatial variability of permafrost properties and simulate the  
133 interactions between permafrost, surface water, and groundwater (Chen et al., 2008;  
134 He et al., 2023; Pomeroy et al., 2022). These models operate on a small-scale basis  
135 and require extensive prior knowledge, following a "bottom-up" approach that relies  
136 on small-scale field observations and situational models to comprehend the effects of  
137 permafrost on hydrology. However, the freeze-thaw cycle is influenced by multiple  
138 interconnected factors, including climate, topography, slope orientation, snowpack,  
139 and vegetation (Chang et al., 2022). The process of upscaling would lead to the  
140 neglect of some variables and the amplification of others (Fenicia and McDonnell,  
141 2022). In contrast, the FLEX-Cryo model is based on the FLEX-Topo-FS model,  
142 which employs a "top-down" modeling procedure that involves observed data  
143 analysis, qualitative perceptual modeling, quantitative conceptual modeling, and the  
144 testing of model realism. This model exhibits the ability to accurately and  
145 expeditiously identify key elements in permafrost hydrological processes and then  
146 simulate hydrology at the catchment scale (Gao et al., 2022).

147 The aim of this study is to integrate the FLEX-Topo-FS model and a glacier  
148 evolution model ( $\Delta h$ -parameterization) to develop a landscape-based model of the



149 mountain cryosphere, referred to as FLEX-Cryo. This model will be utilized to  
150 simulate changes in various components of the mountain cryosphere and evaluate  
151 their impacts on hydrological processes, thereby enhancing our understanding of the  
152 hydrological cycle. The model will be driven by eight bias-corrected Global Climate  
153 Models (GCMs) under SSP2-4.5 and SSP5-8.5 scenarios obtained from the Coupled  
154 Model Intercomparison Project Phase 6 (CMIP6), which will be used to predict future  
155 changes in glaciers, snow, and frozen soil, as well as their effects on hydrology.

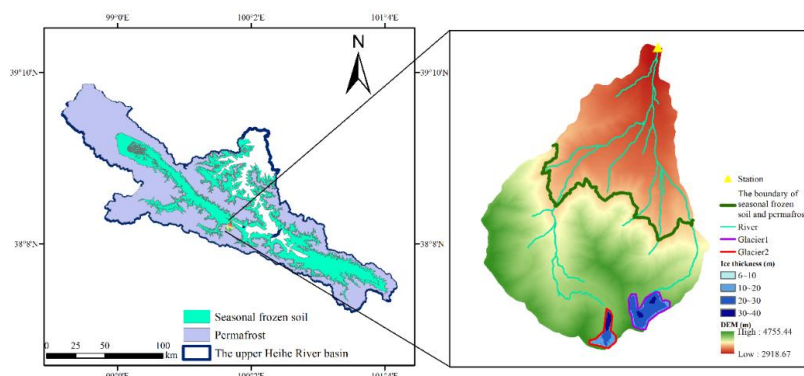
## 156 **2.Study area and data**

### 157 **2.1 Study area**

158 The Hulu catchment is located in the upper reaches of Heihe River basin ( $38^{\circ}$   
159  $12' N$ - $38^{\circ} 17' N$ ,  $99^{\circ} 50' E$ - $99^{\circ} 53' E$ ) and about  $23.1 \text{ km}^2$ . The elevation  
160 ranges from 2960-4820m. The Hulu catchment belongs to continental monsoon  
161 climate. Rainfall is the major phase of precipitation, and there is also snowfall in the  
162 winter. Four landscapes are identified, i.e. glacier (5.6%), alpine desert (53.5%),  
163 vegetation hillslope (37.5%), and riparian zone (3.4%; Fig.2). The landscape pattern  
164 in Hulu catchment has typical altitude zonality. The vegetation and riparian are almost  
165 distributed in the lower elevation bands. Alpine desert, and glacier are in the high  
166 elevation bands. There is almost no human activity in the catchment. There are two  
167 glaciers, i.e. Glacier1 and Glacier2 (Fig.1) in the catchment. And the Glacier1 was  
168 also named as the Shiyi Glacier in the glacier catalogue of China. Seasonal frozen soil  
169 and permafrost both exist in the catchment. The lower limit of permafrost is around in  
170 3650-3700 m. Permafrost region account for 64% of the total catchment and the  
171 others are seasonal frozen soil. The soil generally starts to freeze in the October. Thus  
172 October 1 was set as the start of hydrological year, so forth. All the interannual



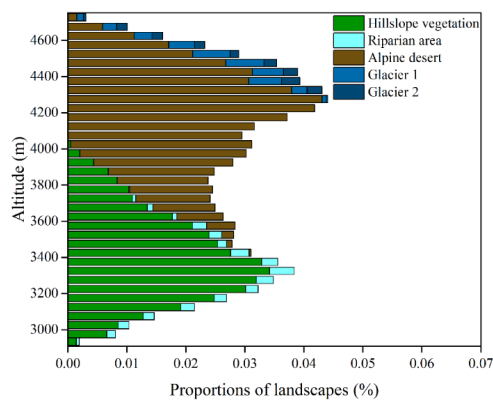
173 variations in this study were based on the hydrology year.



174

175 Figure 1. The digital elevation model, the thickness of glacier and the location of

176 study area



177

178 Figure 2. Landscape classification at different elevation bands

## 179 2.2 Data

180 Temperature and precipitation are observed at 2920 m, near the outlet of the  
181 catchment, from January 1, 2011 to December 31, 2014. Farinotti et al. (2019) used  
182 five models which used the ice flow dynamics to invert ice thickness from surface  
183 features to estimate the ice thickness distribution of about 21500 glaciers outside the  
184 Greenland and Antarctic ice sheets. We used the estimated data for the initial  
185 thickness distribution of Glacier1 and Glacier2 (data download from





186 <https://doi.org/10.3929/ethz-b-000315707>).

187 The Couple Model Intercomparison Project phase 6 (CMIP6) is widely used to  
188 predict future climate. Eight general circulation models (GCMs) (Table 1) under two  
189 climate scenarios (SSP2-4.5 and SSP5-8.5) are used for predicting future climate.  
190 SSP2-4.5 scenario represents medium part of the future pathways, which is usually a  
191 referenced experiment comparing others CMIP6-Endorsed MIPs and it produces a  
192 radiative forcing of  $4.5 \text{ W m}^{-2}$  in 2100. SSP5-8.5 scenario represents the high  
193 emission scenario and it produce a radiative forcing of  $8.5 \text{ W m}^{-2}$  in 2100.

194 There is certain bias in the output of GCMs that needs to be corrected. Firstly,  
195 outputs from eight GCMs under two climate scenarios are interpolated to  $0.5^\circ \times 0.5^\circ$ ,  
196 then the bias corrects are carried out by CMhyd software (download from  
197 <https://swat.tamu.edu/software/cmhyd/>) in which four methods were used including:  
198 distribution mapping of precipitation and temperature, linear scaling of precipitation  
199 and temperature, variance scaling of temperature and local intensity scaling (LOCI) of  
200 precipitation (Teutschbein and Seibert, 2012). The bias-corrected precipitation and  
201 temperature were calculated by using the equal weighted average method to obtain the  
202 multi-model ensemble average values under the SSP2-4.5 and SSP5-8.5 scenarios,  
203 which reduce the uncertainty caused by a single bias correction method and a single  
204 GCM.

205 Table 1. Details of data from eight GCMs used in this study

GCM	Institutions	Grid	Lon. × Lat.
ACCESS-CM2	Australian Community Climate and Earth System Simulator	192×144	1.875°×1.250°
ACCESS-ESM1-5	Australian Community Climate and Earth System Simulator	192×144	1.875°×1.250°



BCC-ECM1	Beijing climate center	320×160	1.125°×1.125°
CMCC-CM2-SR5	Fondazione Centro Euro-Mediterraneo sui Cambiamenti Climatici	288×192	1.25°×0.938°
CMCC-ESM2	Fondazione Centro Euro-Mediterraneo sui Cambiamenti Climatici,	288×192	1.25°×0.938°
GFDL-CM4	National Oceanic and Atmospheric Administration	144×90	2.5°×2°
MPI-ESM1-2-LR	Max Planck Institute for Meteorology	192×96	1.875°×1.875°
NESM3	Nanjing University of Information Science and Technology	192×96	1.875°×1.875°

### 206 3.Methodology

207 The catchment area was divided into 37 elevation bands ranging from 2960 m to  
 208 4820 m, with an interval of 50 m. These elevation bands were classified based on four  
 209 landscapes: glacier, alpine desert, vegetation hillslope, and riparian zone. As a result,  
 210 there were a total of 148 Hydrologic Response Units (HRUs) in the catchment. The  
 211 landscape of alpine desert was the most widespread, covering an elevation range of  
 212 3425 m to 4727 m. The glacier was found in higher altitude areas, specifically  
 213 between the elevation bands of 3725 m and 4727 m.

214 The model parameters used in this study were obtained from a previous study  
 215 conducted in this catchment (Gao et al., 2022). These parameters are listed in Table 2.

216 The  $\Delta h$ -parameterization method was employed, which relies on empirical  
 217 curves that are dependent on the size of the glacier. The study categorized glaciers  
 218 into three size classes: large glacier, area > 20 km<sup>2</sup>; medium-sized glacier, 5 km<sup>2</sup><  
 219 area < 20 km<sup>2</sup>; small glacier, area < 5 km<sup>2</sup>. Both Glacier1 and Glacier2 had areas less



220 than 5 km<sup>2</sup>, making them small glaciers. The glacier mass balance (GMB) was  
221 calculated using the glacier module of the FLEX-Cryo model. The calculated GMB  
222 was then distributed to different elevation bands using the  $\Delta h$ -parameterization  
223 method. Simultaneously, the glacier area and thickness were updated accordingly.  
224 When a glacier was completely melted, the corresponding HRU was transformed into  
225 alpine desert. The evolution of these landscapes was updated every 5 years (Wei et al.,  
226 2023).

227 This study focused on the degradation of glaciers, changes in snow cover and  
228 permafrost, and their impacts on runoff under climate warming. Factors such as solar  
229 radiation, land surface temperatures influenced by snow cover, and vegetation  
230 restoration were not considered. Average annual temperatures and annual precipitation  
231 were used as indicators of future climate change. Glacier thickness at the highest  
232 elevation band and glacier volume were used to quantify the thinning process of  
233 glaciers. The maximum freeze depth of seasonal permafrost, thickness of the active  
234 layer, and freeze-thaw cycle were used to characterize the thawing of frozen soil.  
235 Snow cover days and snow water equivalent were utilized to measure the decreasing  
236 trend of snow. Changes in runoff and runoff coefficient were analyzed to assess the  
237 impact of mountain cryosphere degradation on water resources. Additionally, the  
238 study examined the effect of degradation on runoff yield by observing the low runoff  
239 during the early thaw season and the discontinuation of baseflow recession.

240

241 Table 2. Model parameters and their values or ranges in this study

Parameter	Name	Prior range
$F_{dd}$ (mm °C <sup>-1</sup> d <sup>-1</sup> )	Snow degree day factor	(1.0-5.0)



$C_g$ (-)	Glacier degree factor multiplier	(1.0-3.0)
$S_{U_{max,V}}$ (mm)	Root zone storage in vegetation hillslope	(50-200)
$S_{U_{max,D}}$ (mm)	Root zone storage in alpine desert	(10-100)
$S_{U_{max,R}}$ (mm)	Root zone storage in riparian wetland	(10-100)
$\beta$ (-)	The shape of storage capacity curve	(0-1)
$C_e$ (-)	Soil moisture threshold for reduction of evaporation	(0.1-0.6)
$D$ (-)	Splitter to fast and slow response reservoirs	0.2
$T_{lagf}$ (days)	Lag time from rainfall to peak flow	(0.8-3)
$K_f$ (days)	Fast recession coefficient	(1-10)
$K_s$ (days)	Slow recession coefficient	(10-100)
$k$ (W (m K) <sup>-1</sup> )	Thermal conductivity	2
$\omega$ (-)	Water content as a decimal fraction of the dry soil weight	0.12
$\rho$ (kg/m <sup>3</sup> )	Bulk density of the soil	1000
Pcalt	Precipitation increasing rate	4.2
Tcalt	Temperature lapse rate	0.68

### 242 3.1 FLEX-Cryo model

243 FLEX-Cryo model is a landscape-based cryospheric hydrological model, which  
 244 considers multi-elements of cryosphere and their impacts on hydrology, including  
 245 glacier, snow and frozen soil. The elevation is also an important factor affecting the  
 246 temperature and precipitation. The temperature and precipitation are interpolated  
 247 based on the band in situ observation (2980 m). the temperature regression rate is -  
 248 0.68°C/100m and the precipitation increasing rate is 4.2%/100m. The value of 0 °C is  
 249 the threshold temperature to split snowfall ( $P_s$ ) and rainfall ( $P_l$ ).



### 250 **3.1.1 Glacier and snow module**

251 Glacier and snow melt were both calculated by the temperature - index method  
252 which is on basis of the degree-day factor  $F_{dd}$  ( $\text{mm } ^\circ\text{C}^{-1} \text{d}^{-1}$ ) ( $F_{dd}$  in Table 2; equation  
253 (11) in Table 3). Due to the lower albedo, the degree-day of ice is greater than snow,  
254 and multiplied by a coefficient  $C_g$  ( $C_g$  in Table 2; equation (9) in Table 3). The glacier  
255 area runoff  $Q_g$  is calculated through the linear reservoir  $S_g$  which the liquid rain  $P_l$  and  
256 glacier melt  $M_g$  inflow and the runoff outflow ((Equation (4) in Table 3) and a  
257 recession parameter  $K_{fg}$  (Equation (1) in Table 3).

### 258 **3.1.2 Frozen soil module**

259 The Stefan equation was calculated at the different elevation bands based on the  
260 interpolated temperature (Equation (18) in Table 3). The observed temperature was  
261 multiplied by 0.6 to translate the air temperature to ground temperature which was  
262 required in the equation. In this equation, the  $\varepsilon$  is the freeze / thaw depth (m),  $k$  is the  
263 thermal conductivity ( $2 \text{ W (m K)}^{-1}$ ),  $F$  is the freeze / thaw index ( $^\circ\text{C}$ ) which represents  
264 the cumulative value of the temperature below (above)  $0^\circ\text{C}$ ,  $Q_L$  is the volumetric  
265 latent heat of soil ( $\text{J m}^{-3}$ ),  $L$  is the latent heat of the fusion of ice ( $3.35 \times 10^5 \text{ J kg}^{-1}$ ),  
266  $\omega$  is the water content as a decimal fraction of the dry soil weight (0.12), and  $\rho$  is the  
267 bulk density of the soil ( $1000 \text{ kg m}^{-3}$ ).

268 The frozen soil impacts on the runoff by the soil water and groundwater. In the  
269 frozen season, the baseflow comes merely from the groundwater discharge at the  
270 supra-permafrost layer ( $Q_s$ ). In the freezing season, when the freeze depth is greater  
271 than 3 m and the supra-permafrost groundwater is frozen. And due to certain amount  
272 of unfrozen water in frozen soil, the volume of slow reservoir  $S_s$  (Equation (19) and  
273 (20)) will be reduced to 10%. The groundwater system in seasonal frozen soil region



274 is still connected in winter. When the soil completely thaws at the lowest elevation  
275 band, the runoff generated by the frozen  $S_s$  will rapidly release to the  $Q_s$ . The  
276 baseflow generation is assumed to be a linear recession process. The generated  
277 baseflow is controlled by the reservoir  $S_s$ , recession coefficient  $K_s$ , the time  $t$  and  
278 initial runoff  $Q_0$  (Equation (21)).

$$279 \quad \frac{dS_s}{dt} = R_s - Q_s - F_s \quad (19)$$

$$280 \quad F_s = \begin{cases} 0.9 \cdot S_s & \varepsilon \geq 3m \\ -0.9 \cdot S_s & \text{completely thaw} \end{cases} \quad (20)$$

$$281 \quad Q = Q_0 \cdot e^{-t/K_s} \quad (21)$$

### 282 3.1.3 Rainfall-runoff module

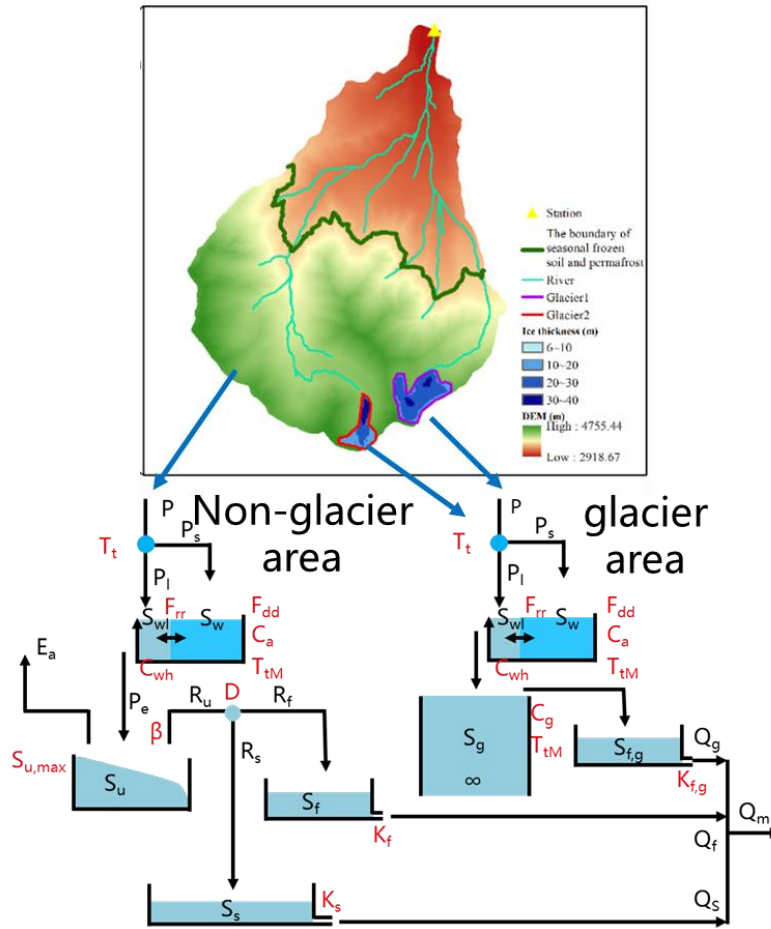
283 The root zone reservoir  $S_u$  (equation (6) in Table 3), fast response reservoir  $S_f$   
284 (equation (7) in Table 3) and slow reservoir  $S_s$  (equation (8) in Table 3) are critical  
285 reservoirs for simulating rainfall-runoff processes. The runoff yield process is  
286 governed by the root storage capacity and the water input to the soil (equation (12) in  
287 Table 3) meanwhile the actual evaporation is determined by soil moisture and  
288 potential evaporation. The generation runoff flows into two linear reservoirs ( $S_f$  and  
289  $S_s$ ) which represents the storm flow ( $Q_f$ ) and groundwater runoff ( $Q_s$ ), respectively.  
290 The runoff yield process has similarity in alpine desert, vegetation hillslope and  
291 riparian zone and the difference is the root zone storage capacity ( $S_{u\max}$ ). In the  
292 vegetation hillslope, plants have well-developed root systems and the root zone has a  
293 larger storage capacity. So, the  $S_{u\max-V}$  was set with larger value. For the alpine desert  
294 and riparian zone, the  $S_{u\max-D}$  and  $S_{u\max-R}$  were both limited due to the less developed  
295 root system and storage capacity.



296 Table 3. The FLEX-Cryo model equations

Landscape	Runoff equation	Water balance equation	Structural equation
Glacier	$Q_g = \frac{S_g}{K_{fg}} \quad (1)$	$\frac{dS_g}{dt} = P_l + M_g - Q_g \quad (4)$	$M_g = \begin{cases} F_{dd} \cdot T \cdot C_g & S_w = 0 \text{ and } T > 0 \\ 0 & S_w > 0 \text{ and } T \leq 0 \end{cases} \quad (9)$ $\Delta h = (h_t - 0.30)^2 + 0.60(h_t - 0.30) + 0.09 \quad (10)$
Alpine desert	$Q_t = \frac{S_f}{K_f} \quad (2)$	$\frac{dS_w}{dt} = P - M_w \quad (5)$	$M_w = \begin{cases} F_{dd} \cdot T & T > 0 \\ 0 & T \leq 0 \end{cases} \quad (11)$ $R_U = (P_l + M_w) \cdot \left( 1 - \left( 1 - \frac{S_U}{S_{U_{max}}} \right)^\beta \right) \quad (12)$
Hillslope vegetation		$\frac{dS_u}{dt} = P_l + M_w - E_a - R_u \quad (6)$	$E_a = E_p \cdot \left( \frac{S_U}{C_e \cdot S_{U_{max}}} \right) \quad (13)$ $R_f = R_U \cdot D \quad (14)$ $R_s = R_U \cdot (1 - D) \quad (15)$
Riparian area		$\frac{dS_f}{dt} = R_f - Q_f \quad (7)$	$R_f(t) = \sum_{i=1}^{T_{logf}} c_f(i) \cdot R_f(t - i + 1) \quad (16)$ $c_f(i) = \frac{i}{T_{logf}} \quad (17)$ $\sum_{u=1}^u$
	$Q_s = \frac{S_s}{K_s} \quad (3)$	$\frac{dS_s}{dt} = R_s - Q_s \quad (8)$	$\varepsilon = \left( \frac{2 \cdot 86400 \cdot k \cdot F}{Q_L} \right)^{0.5} = \left( \frac{2 \cdot 86400 \cdot k \cdot F}{L \cdot \omega \cdot \rho} \right)^{0.5} \quad (18)$

297



298

299 Figure.3 Structure of the FLEX-Cryo model. The abbreviation in red color

300 indicates paraments and the abbreviations in black indicate storage components and

301 fluxes.

302 **4. Results**

303 **4.1 Future climate change**

304 Figure 4 shows the prediction of future climate in 2015-2100 under the SSP2-4.5

305 and SSP5-8.5 scenarios based on the average values of eight climate models (adjusted

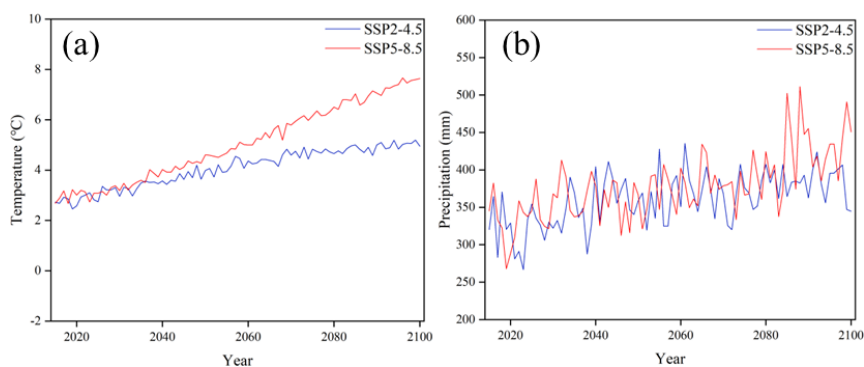
306 for bias). According to the SSP2-4.5 scenario, the temperature will increase by 2.07°C

307 relatively steadily by 2100. Under the SSP5-8.5 scenario, temperatures are projected





308 to continue to rise by  $5.04^{\circ}\text{C}$  over the course of the century. Precipitation changes are  
309 more drastic than temperature, especially after the eighties of the 21st century under  
310 the SSP5-8.5 scenario. Overall, the precipitation under the SSP2-4.5 scenario  
311 increased by 14.25 %, and the precipitation increased by 33.50 % under the SSP5-8.5  
312 scenario. Before the 80s of the 21st century, the increase in precipitation was almost  
313 the same under different scenarios, about  $8.9\text{ mm }10\text{ years}^{-1}$  and  $8.5\text{ mm }10\text{ years}^{-1}$ ,  
314 respectively.



315  
316 Figure 4. The annual average temperature (a) and annual precipitation mean (b) of  
317 bias adjusted multi-Global Climate Model from 2015-2100.

#### 318 **4.2 Predicting glacier retreat**

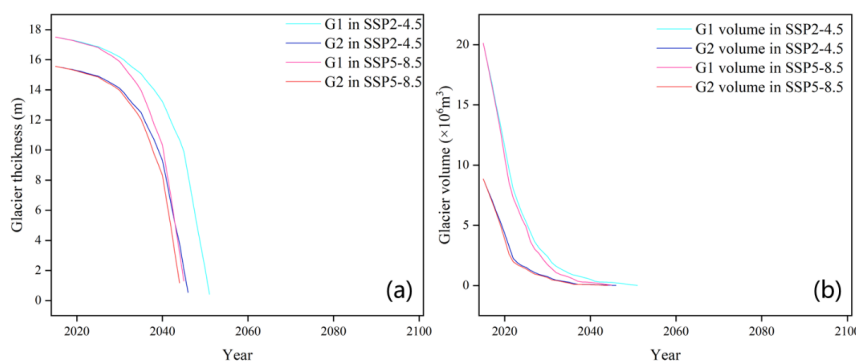
319 In the initial status (Figure 5), the Glacier1 and Glacier2 had areas of  $8.78 \times 10^5$   
320  $\text{m}^2$  and  $4.08 \times 10^5 \text{ m}^2$ , and ice volumes of  $20.13 \times 10^6 \text{ m}^3$  and  $8.86 \times 10^6 \text{ m}^3$ , respectively.  
321 Glacier1 exhibited greater thickness and volume compared to Glacier2.

322 Both Glacier1 and Glacier2 experienced retreat, characterized by a decrease in  
323 glacier volume and thinning of glacier thickness (Figure 5). Starting from the 2020s,  
324 the glacier volume showed a rapid decline, and after the 2030s, the highest-altitude  
325 portion of the glacier entered a phase of rapid thinning. Around 2040, the glacier  
326 degradation reached a stabilization period, during which glaciers were only present in



327 the highest elevation band. According to the SSP2-4.5 scenario, Glacier1 and Glacier2  
328 are projected to completely melt and disappear by 2051 and 2046, respectively. Under  
329 the SSP5-8.5 scenario, the complete melt-out time is slightly earlier, occurring in  
330 2045 and 2044 for Glacier1 and Glacier2, respectively. After the glaciers completely  
331 melt, approximately 5.6% of the ablated glacier area will transform into alpine desert.

332 Taking the glacier changes in 2025, 2035, and 2045 as examples, under the  
333 SSP2-4.5 scenario, the area of Glacier1 is projected to decrease to  $5.49 \times 10^5 \text{ m}^2$ ,  
334  $1.52 \times 10^5 \text{ m}^2$ , and  $0.26 \times 10^5 \text{ m}^2$ , with corresponding volume reductions to  $5.27 \times 10^6$   
335  $\text{m}^3$ ,  $1.03 \times 10^6 \text{ m}^3$ , and  $0.26 \times 10^6 \text{ m}^3$ , respectively (Figure 7). Comparatively, the retreat  
336 trend is more pronounced under the SSP5-8.5 scenario. The area of Glacier1 is  
337 projected to be  $4.00 \times 10^5 \text{ m}^2$ ,  $0.81 \times 10^5 \text{ m}^2$ , and  $0.26 \times 10^5 \text{ m}^2$ , with volumes of  
338  $4.86 \times 10^6 \text{ m}^3$ ,  $0.71 \times 10^6 \text{ m}^3$ , and  $0.03 \times 10^6 \text{ m}^3$ , respectively. The degradation of  
339 Glacier2 follows a similar pattern to that of Glacier1, except that Glacier2 experiences  
340 less ice loss. According to the SSP5-8.5 scenario, Glacier2 is projected to completely  
341 melt by 2045. In 2025 and 2035, the area of Glacier2 remains consistent, with values  
342 of  $1.67 \times 10^5 \text{ m}^2$  and  $0.51 \times 10^5 \text{ m}^2$  for both scenarios, respectively. These glaciers are  
343 only distributed within the elevation bands from 4625 m to 4727 m and from 4675 m  
344 to 4727 m.



345



346 Figure 5. The glacier thickness (a) and glacier volume (b) change from 2015 to  
347 2100 for the Glacier1 and Glacier 2

### 348 **4.3 Forecasting the degradation of frozen soil**

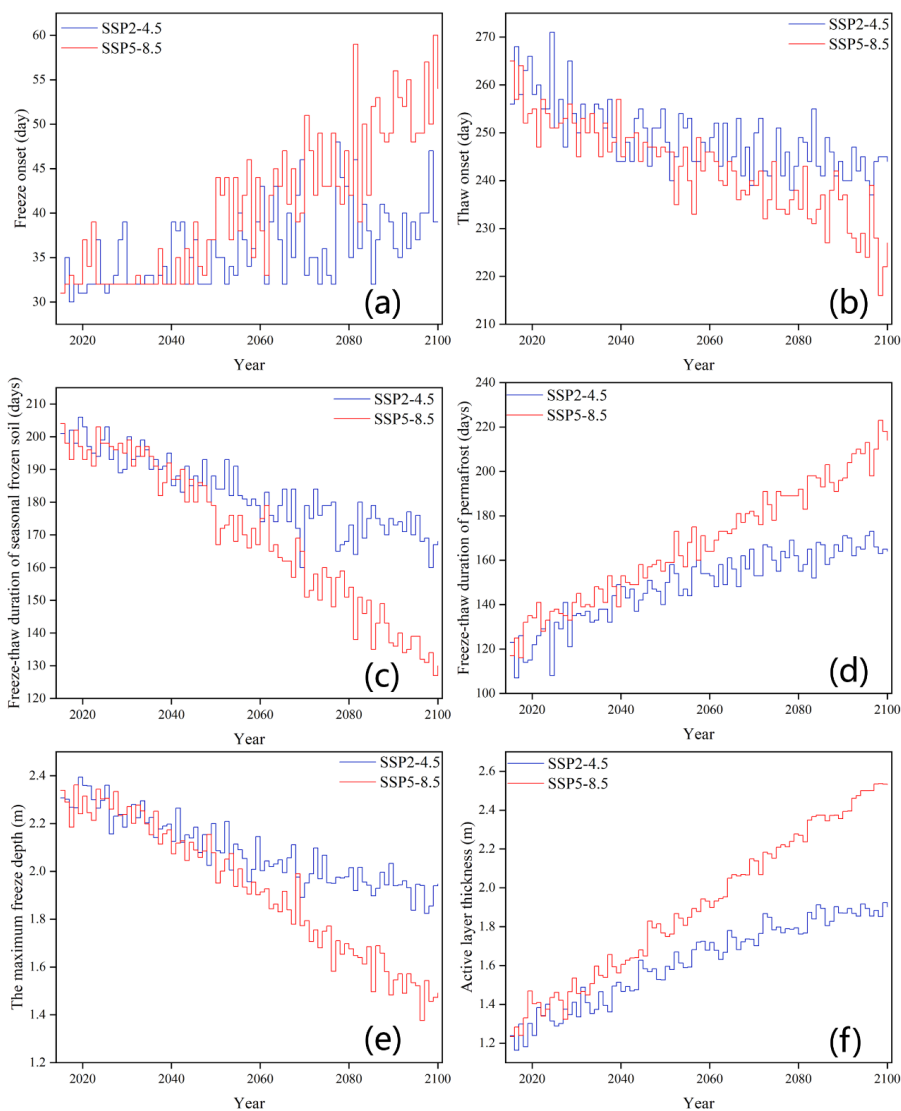
349 In the initial state (Figure 6), the seasonal frozen soil exhibited an early freeze  
350 onset in early November, with a freeze duration of approximately 200 days at the  
351 lowest elevation band. The permafrost, on the other hand, experienced a thaw onset in  
352 mid-June, lasting around 120 days at the highest elevation band. The maximum freeze  
353 depth was approximately 2.30 m at lower altitudes, while the active layer thickness  
354 measured around 1.27 m at the highest elevation.

355 By the end of the 21st century, under the SSP2-4.5 scenario, several changes are  
356 projected to occur. The freeze onset of seasonal frozen soil will be delayed by 10  
357 days, resulting in a shortened freeze-thaw cycle duration of approximately 1 month.  
358 The thaw onset of permafrost will be advanced by 19 days, leading to an increased  
359 freeze-thaw cycle duration of nearly 50 days. Additionally, the maximum freeze depth  
360 is expected to decrease by 5.17 cm per decade, while the active layer thickness will  
361 increase by approximately 8.24 cm per decade. The degradation trend of permafrost is  
362 more severe under the SSP5-8.5 scenario. By the end of the 21st century, compared to  
363 the SSP2-4.5 scenario, the freeze onset of seasonal frozen soil will be shortened by 22  
364 days, resulting in a further reduction of the freeze-thaw cycle duration by over 2  
365 months. The thaw onset of permafrost will occur approximately 1 month earlier, and  
366 the freeze-thaw cycle duration of permafrost will increase by nearly 3 months. The  
367 decreasing trend of the maximum freeze depth and the increasing trend of the active  
368 layer thickness are approximately twice as pronounced under the SSP5-8.5 scenario  
369 compared to the SSP2-4.5 scenario. While the freeze onset of seasonal frozen soil



370 exhibits significant variation between consecutive years, the other frozen soil  
371 elements follow a more stable change pattern. Before 2040, there is little difference  
372 between the two scenarios, except for the active layer thickness. Seasonal frozen soil  
373 will begin to freeze around mid-November and late November, while permafrost will  
374 start to thaw in mid-May and early June by the year 2100.

375 Under the SSP2-4.5 and SSP5-8.5 scenarios, the lower limit of permafrost  
376 gradually expands along the altitudinal gradient, with rates of 4.30 m per year and  
377 8.75 m per year, respectively (Figure 7). In the SSP2-4.5 scenario, the lower limit of  
378 permafrost is projected to reach altitudes of 3685 m, 3795 m, 3835 m, 3865 m, 3985  
379 m, and 4015 m in the years 2025, 2035, 2045, 2055, 2075, and 2095, respectively. The  
380 lower limit of permafrost in 2095 under the SSP2-4.5 scenario is comparable to the  
381 lower limit of permafrost (3965 m) in 2055 under the SSP5-8.5 scenario. Before 2045,  
382 the lower bound exhibits similar changes under both scenarios, but a significant  
383 divergence occurs afterward. The lower limit is projected to increase to 4355 m by  
384 2095 under the SSP5-8.5 scenario.



385

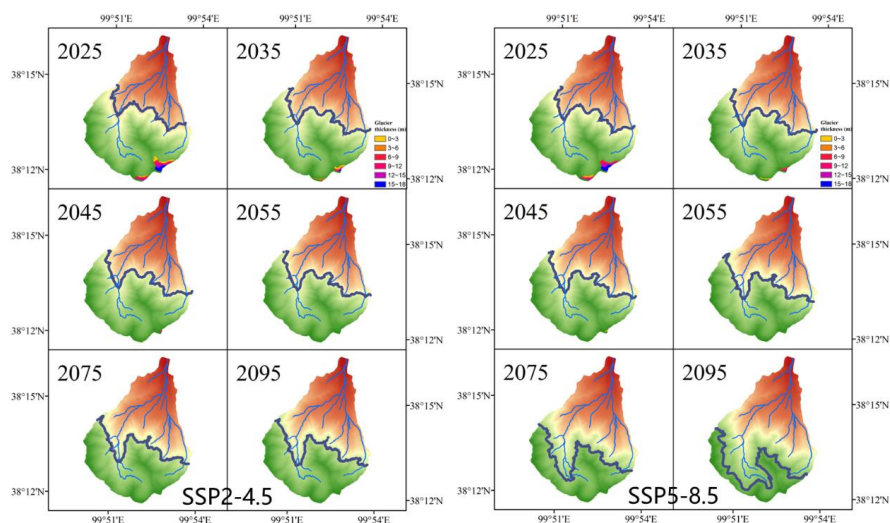
386 Figure 6. Changes in seasonal frozen soil and permafrost from 2015-2100 under

387 SSP2-4.5 and SSP5-8.5 scenarios. (a, b) Freeze and thaw onset. (c, d) Freeze-Thaw

388 duration of frozen soil and permafrost. (e, f) The maximum freezing depth and active

389 layer thickness.

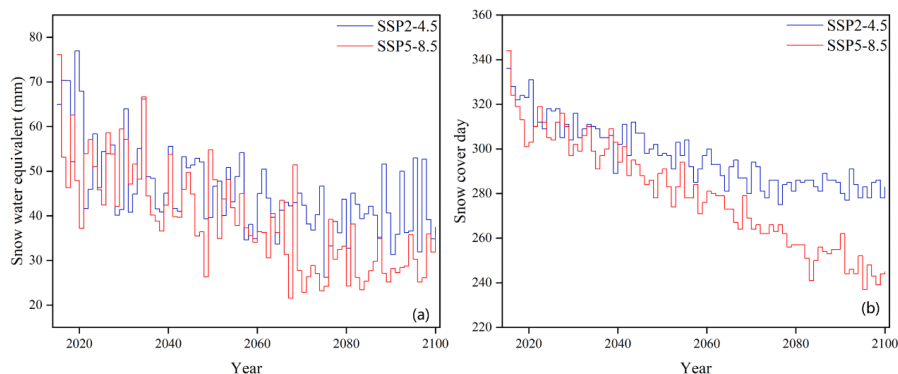
390



391  
392 Figure 7. Changes of ice thickness and the lower limit of permafrost in 2025, 2035,  
393 2045, 2055, 2075 and 2095 under SSP2-4.5 and SSP5-8.5.

#### 394 4.4 Snow change in the future

395 The duration of snow cover is projected to decrease continuously in the future.  
396 Under the SSP2-4.5 scenario, the snow cover days are likely to be shortened by 45  
397 days, while under the more severe SSP5-8.5 scenario, the reduction is expected to be  
398 around 76 days. Simultaneously, the snow water equivalent, which measures the  
399 amount of water contained in the snowpack, is projected to exhibit more variable  
400 changes but with an overall decreasing trend. For the SSP2-4.5 scenario, the snow  
401 water equivalent will decrease by 0.24 mm per year, resulting in a reduction of  
402 approximately 41.4%. Under the SSP5-8.5 scenario, the decrease in snow water  
403 equivalent is more pronounced, with a drop of 0.35 mm per year, corresponding to a  
404 reduction of up to 46.0%.



405  
406 Figure 8. (a) snow water equivalent at entire watershed and (b) snow cover day at  
407 the highest band.

#### 408 4.5 Project future runoff

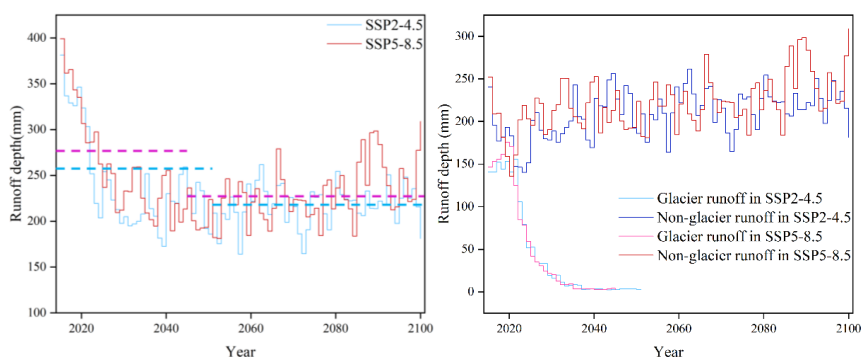
409 The depth of runoff in the entire basin shows a declining trend in the future.  
410 Under both the SSP2-4.5 and SSP5-8.5 scenarios, before the complete melting of  
411 glaciers, the runoff depth is estimated to be around 257 mm and 277 mm, respectively.  
412 After the glaciers completely melt, the runoff depth is projected to decrease by  
413 15.56% and 18.05% for the SSP2-4.5 and SSP5-8.5 scenarios, respectively (Figure 9).  
414 By 2100, the average annual runoff depth is expected to be similar for both scenarios,  
415 at approximately 217 mm and 227 mm. In the SSP2-4.5 and SSP5-8.5 scenarios, the  
416 tipping point for the runoff depth in the glacier area is projected to occur in 2021 and  
417 2019, respectively, with values of 155.93 mm and 175.98 mm. After reaching the  
418 tipping point, the runoff depth in the glacier area is likely to continue decreasing until  
419 the glaciers completely melt. In non-glacier areas, the runoff depth shows an increase  
420 of 0.48 mm per year and 0.65 mm per year.

421 The runoff coefficient, which represents the proportion of precipitation that  
422 becomes runoff, follows a similar pattern to the glacier runoff changes. It initially  
423 increases, then decreases, and eventually reaches a relatively stable state after the



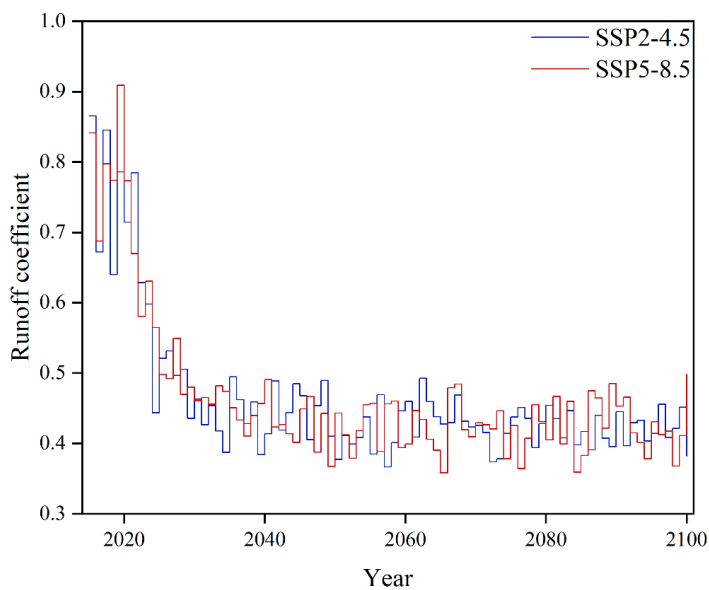
424 glaciers completely melt (Figure 10). The maximum values of the runoff coefficient  
425 occur in 2021 and 2019, coinciding with the tipping points of the glacier runoff. By  
426 the end of the 21st century, the runoff coefficient is projected to be dramatically  
427 reduced to approximately 0.42.

428 Two hydrological phenomena observed in permafrost mountainous catchments,  
429 namely the low runoff in the early thawing season (LRET) and discontinuous  
430 baseflow recession (DBR) (Gao et al., 2022), are expected to persist in the future  
431 (Figure 11). Meanwhile, baseflow, which represents the sustained flow of water from  
432 groundwater, shows an increasing trend. The duration of the early thawing season is  
433 projected to be further reduced. The first recession coefficient remains unchanged,  
434 while the second recession coefficient progressively increases. Under the SSP2-4.5  
435 scenario, the second recession coefficient is equal to 74 days, which is consistent with  
436 the recession coefficient in 2060 under the SSP5-8.5 scenario. This suggests that the  
437 permafrost area undergoes less significant changes under SSP2-4.5 scenario than  
438 SSP2-8.5 scenario according to Figure 7. The baseflow gradually increases, especially  
439 in the SSP5-8.5 scenario, as indicated by the runoff depth on a logarithmic scale.



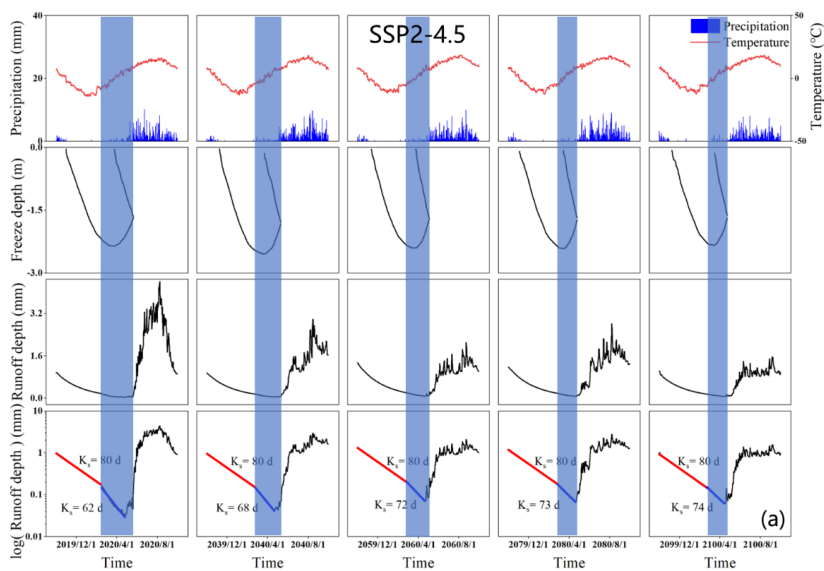
440  
441 Figure 9. (a) The predicted runoff depth of the total basin (b) Runoff in the glacier and  
442 in the non-glacier from 2015-2100



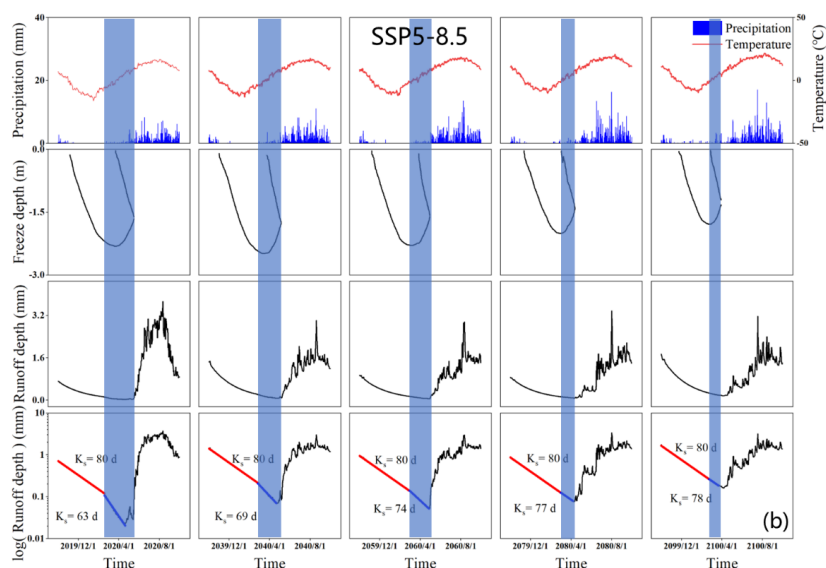


443

444 Figure 10. Project runoff coefficient under SSP2-4.5 and SSP5-8.5 scenarios.



445



446

447 Figure 11. Temperature, precipitation, runoff depth and freeze-thaw cycle in 2020,  
448 2040, 2060, 2080 and 2100 under SSP2-4.5 (a) and SSP5-8.5 scenarios (b).

## 449 5. Discussion

### 450 5.1 Changes of the mountain cryosphere in future

451 The cryosphere, which encompasses glaciers, snow, frozen soil, and permafrost,  
452 plays a vital role in storing approximately 75% of the world's freshwater resources,  
453 while around 17% of the global population resides in cryosphere regions (Qin et al.,  
454 2021). Understanding the changes occurring in the cryosphere is crucial for assessing  
455 the long-term sustainability of water resources (Whitfield et al., 2021). The Hulu  
456 catchment, located in the northeast Tibet Plateau, exhibits a diverse distribution of  
457 cryosphere elements, making it an ideal area for studying these changes (Gao et al.,  
458 2019; Xu et al., 2019). However, there is a lack of research on the degradation of  
459 multiple cryosphere elements within the Hulu catchment and its implications for



460 future hydrology, despite the Heihe River Basin being recognized as a typical region  
461 for studying hydrological and water resource changes in cold regions (Ning et al.,  
462 2008). In this study, we projected a future warming trend of 0.3°C per decade and  
463 0.6°C per decade, accompanied by an increase in precipitation of 7.9 mm per decade  
464 and 12.0 mm per decade under the SSP2-4.5 and SSP5-8.5 scenarios, respectively  
465 (Figure 4). These projections align with the findings of Chen et al. (2022), who  
466 observed similar warming trends of 0.3-0.4 °C per decade and 0.7-0.8°C per decade,  
467 as well as precipitation increases ranging from 1.6-14.8 mm per decade and 6.0-20.6  
468 mm per decade under similar scenarios. This consistency between our projections and  
469 previous research supports the reliability of the forcing data used in the FLEX-Cryo  
470 model.

471 Furthermore, Wang et al. (2018) predicted an increase in the annual maximum  
472 freeze depth in the Heihe River Basin from 2011 to 2066 at a rate of 5.4 cm per  
473 decade, which closely aligns with the predicted change of 5.2 cm per decade in our  
474 study (Figure 6). While there have been limited studies investigating future changes in  
475 glaciers and other cryosphere elements within the Hulu catchment, including the Shiyi  
476 Glacier, conducting a comparative analysis with projections from other regions can  
477 enhance our understanding of mountain cryosphere retreat. Although the comparative  
478 analysis approach may have some limitations in terms of rigor, it provides valuable  
479 insights (Han et al., 2023).

## 480 **5.2 The effect of the mountain cryosphere degradation on runoff**

481 Glaciers and snow cover play a crucial role in water retention, with meltwater  
482 contributing significantly to downstream water resources and the ecological  
483 environment (Stecher et al., 2023). The turning point of glacier runoff represents a



484 critical tipping point that signifies not only the thinning of glaciers but also the  
485 irreversible stage of water resources in the basin (Brovkin et al., 2021). In the Hulu  
486 catchment, the proportion of glacier runoff reached 51% to 55% between 2019 and  
487 2021, indicating that it is in the turning point period (Figure 9). Subsequently, the  
488 contribution of glacier runoff gradually decreases until complete melting occurs.  
489 Temperature is the primary factor influencing glacier runoff, while precipitation and  
490 temperature together determine the proportion of glacier runoff in relation to total  
491 runoff. Although the highest contribution of glacier runoff and the tipping point of  
492 glacier runoff may not align precisely, after the tipping point, the capacity of glacier  
493 runoff to contribute to overall runoff continuously diminishes. From 2015 to 2021,  
494 there has been a decreasing trend in precipitation, leading to a corresponding decline  
495 in non-glacier runoff (Figure 4 and 9). Thus, while glacier runoff has increased, the  
496 total runoff has decreased. However, between 2032 and 2038, even though rainfall  
497 continues to decline, the contribution of glacier runoff to overall runoff becomes  
498 negligible due to the limited volume of ice remaining (glacier volume  $< 1 \times 10^6 \text{ m}^3$ ),  
499 resulting in minimal glacier melting runoff (Figure 5 and Figure 9). On the other  
500 hand, once the glaciers have completely melted, the total runoff in the Hulu catchment  
501 is reduced by 16% to 18%, and the runoff coefficient is halved (Figure 9 and Figure  
502 10). This highlights the critical role of glaciers as solid freshwater reservoirs in  
503 regulating water sources and mitigating droughts (McCarthy et al., 2022).

504 The freeze-thaw cycle has a significant impact on runoff yield and hydrological  
505 response routines in the Hulu catchment (Sun et al., 2022; Wang et al., 2020).  
506 Precipitation in the Hulu catchment is primarily concentrated in the summer when soil  
507 moisture is high and even close to saturation, making saturation excess flow the main



508 mechanism for runoff generation (Li et al., 2016). During the freeze-thaw cycle, the  
509 weak permeability of frozen soil affects both surface runoff and infiltration. Soil  
510 runoff primarily occurs through underground in hillslope and surface water flow in  
511 riparian area, resulting in a faster response to rainfall and snowmelt and contributing  
512 to a higher runoff coefficient (Hu et al., 2022; Jones et al., 2023). However, it is  
513 important to note that shallow frozen soil does not completely block the interaction  
514 between deeper soil layers and the surface. Frost heave in the soil creates large pores,  
515 allowing snowmelt water and precipitation to bypass the matrix layer and reach the  
516 deeper soils (Jiang et al., 2021; Zhang et al., 2023). This phenomenon is considered  
517 one of the significant reasons for low runoff in the early thawing season (Mohammed  
518 et al., 2021). Low runoff is observed between the frozen season and complete thawing  
519 season (Figure 11). The duration of freeze-thaw cycles in seasonal frozen soils is  
520 shortening, and freeze onset is being delayed due to the warming climate, resulting in  
521 a decreasing duration of low runoff. However, the temperature during the freezing  
522 season remains lower than the initial frost heave temperature of the soil, and there is  
523 still a deficit of soil water in the early thaw, indicating that the prevalence of low  
524 runoff will persist in the future (Teng et al., 2022; Wen et al., 2024).

525 The freezing state has a significant impact on the recession process of baseflow,  
526 and permafrost plays a crucial role in discontinuous baseflow (Cooper et al., 2023; J.  
527 Wang et al., 2022). During the freezing season, baseflow follows a linear recession  
528 process ( $K_s = 80$  days), with contributions from both permafrost and seasonal frozen  
529 soil regions (Figure 11). In the frozen season, the groundwater under the supra-  
530 permafrost layer becomes inactive, and baseflow is solely derived from the seasonal  
531 frozen soil regions, causing a discontinuous recession. With climate warming, the



532 lower limit of permafrost gradually moves upward along the elevation, resulting in the  
533 shrinking of the permafrost region. This suggests that in the future, an increased  
534 proportion of baseflow will originate from the expanding area of seasonal frozen soil,  
535 leading to a gradual decrease in the influence of permafrost on baseflow.  
536 Consequently, the discontinuous recession of baseflow will gradually transition into a  
537 linear recession. Furthermore, an increase in the thickness of the active layer enhances  
538 the soil water storage capacity, contributing to a gradual rise in baseflow (Yao et al.,  
539 2021).

### 540 **5.3 Uncertainty and limitations**

541 The uncertainty in this study arises from the forcing data of the General  
542 Circulation Models (GCMs), the bias correction methods, and the parameters selected  
543 in the FLEX-Cryo model (Wilby and Harris, 2006). The coarse spatial resolution of  
544 the GCMs prevents a comprehensive description of the climate at the basin scale,  
545 particularly in plateau and mountainous regions heavily influenced by altitude. The  
546 selection of parameters for the FLEX-Cryo model is also a significant source of  
547 uncertainties. Due to the complex topography in the mountain cryosphere, degree-day  
548 factor, altitude effect on climate and soil water storage capacity cannot be fully  
549 reflected at the catchment scale. To mitigate some of the uncertainties associated with  
550 the GCM outputs, a multi-model and multi-method approach is employed in this  
551 study. The equal weighted average method is used to combine the values from  
552 different models and methods, aiming to reduce uncertainties and provide a more  
553 robust assessment of the results. It is important to note that the optimal parameter  
554 group selected for the FLEX-Cryo model in this study has been chosen based on  
555 previous research (Gao et al., 2022). While this helps to establish a more reliable



556 parameterization, there may still be inherent limitations in the chosen parameter  
557 values. Overall, the uncertainties and limitations associated with the forcing data, bias  
558 correction methods, and parameter selection in the FLEX-Cryo model need to be  
559 considered when interpreting the results of this study. Further research and  
560 improvements in these areas can enhance the accuracy and reliability of future  
561 assessments of the effects of mountain cryosphere degradation on runoff.

## 562 **6.Conclusions**

563 The mountain cryosphere, encompassing glaciers, snow, and frozen soil, plays a  
564 critical role in downstream water resources and the ecological environment.  
565 Understanding its response to climate change is crucial for effective water resource  
566 management and flood prevention. In this study, we employed the FLEX-Cryo model  
567 and data from eight Global Climate Models (GCMs) under the SSP2-4.5 and SSP5-  
568 8.5 scenarios to project the potential impacts of climate change on the mountain  
569 cryosphere and hydrology. Based on our simulation results, the following conclusions  
570 can be drawn:

571 (1) The air temperature is projected to increase by 2.1 °C and 5 °C by 2100,  
572 while precipitation is expected to increase by 8 mm/10 years and 12 mm/10 years.  
573 These changes in temperature and precipitation patterns indicate a significant shift in  
574 the climatic conditions of the study area.  
575 (2) Glacier and snow cover are anticipated to experience retreat and shrinkage in the  
576 future. Under the SSP5-8.5 and SSP2-4.5 scenarios, glaciers are projected to  
577 completely melt by 2045 and 2051, respectively. Additionally, the duration of snow  
578 cover will be shortened by 45 days and 76 days, while the snow water equivalent will  
579 decrease by 0.24 mm/yr and 0.35 mm/yr.



580 (3) The frozen soil is expected to undergo degradation. By 2100, the freeze onset of  
581 seasonal frozen soil is projected to delay by 10 days and 22 days, and the thaw onset  
582 of permafrost is expected to advance by 19 days and 32 days. The lower limit of  
583 permafrost is estimated to reach altitudes of 4015 m and 4355 m along the altitudinal  
584 gradient. Moreover, the maximum freeze depth will decrease by approximately 5.17  
585 cm/10 years and 10.93 cm/10 years, while the active layer thickness will increase by  
586 8.24 cm/10 years and 15.47 cm/10 years.

587 (4) The degradation of the mountain cryosphere has significant implications for water  
588 resources in the catchment area, particularly in terms of runoff yield. The tipping  
589 point for glacier runoff occurred between 2019 and 2021. Once the glaciers have  
590 completely melted, the depth of runoff is projected to decrease by approximately 16%  
591 and 18%. However, in non-glacier areas, the depth of runoff is expected to increase by  
592 0.22 mm/yr and 1.07 mm/yr from 2015 to 2100. By the end of the 21st century, the  
593 runoff coefficient in the catchment is projected to reach approximately 0.42.

594 Importantly, the duration of low runoff during the early thawing season will be  
595 shorter. The discontinuous recession of baseflow is gradually transitioning towards a  
596 linear pattern, resulting in increased baseflow. The second recession coefficients are  
597 estimated to be around 74 days and 78 days, respectively, by the year 2100.

598 In conclusion, this study provides insights into the potential impacts of climate change  
599 on the mountain cryosphere and hydrology. The projected changes in temperature,  
600 precipitation, glacier retreat, snow cover, and frozen soil dynamics highlight the  
601 urgent need for proactive water resource management strategies in the face of a  
602 changing climate. Further modelling research and monitoring efforts are necessary to  
603 refine these projections and guide effective adaptation measures to sustainably





604 manage water resources in mountainous regions.

605

606 **Competing interests**

607 At least one of the (co-)authors is a member of the editorial board of Hydrology and  
608 Earth System Sciences.

609

610 **Acknowledgements**

611 This research has been supported by the National Natural Science Foundation of  
612 China (grant no. 42071081 and 42122002). Zheng Duan acknowledges the support  
613 from the Crafoord Foundation (No. 20210552).

614

615 **References**

- 616 Abdelhamed, M. S., Elshamy, M. E., Wheeler, H. S., and Razavi, S.: Hydrologic-land  
617 surface modelling of the Canadian sporadic-discontinuous permafrost:  
618 Initialization and uncertainty propagation, *Hydrol. Process.*, 36,  
619 <https://doi.org/10.1002/hyp.14509>, 2022.
- 620 Adler, C., Huggel, C., Orlove, B., and Nolin, A.: Climate change in the mountain  
621 cryosphere: impacts and responses, *Reg Environ Change*, 19, 1225–1228,  
622 <https://doi.org/10.1007/s10113-019-01507-6>, 2019.
- 623 Andrianaki, M., Shrestha, J., Kobierska, F., Nikolaidis, N. P., and Bernasconi, S. M.:  
624 Assessment of SWAT spatial and temporal transferability for a high-altitude  
625 glacierized catchment, *Hydrol. Earth Syst. Sci.*, 23, 3219–3232,  
626 <https://doi.org/10.5194/hess-23-3219-2019>, 2019.
- 627 Arendt, A., Krakauer, N., Kumar, S. V., Rounce, D. R., and Rupper, S.: Editorial:  
628 Collaborative Research to Address Changes in the Climate, Hydrology and  
629 Cryosphere of High Mountain Asia, *Front. Earth Sci.*, 8, 605336,  
630 <https://doi.org/10.3389/feart.2020.605336>, 2020.



- 631 Blöschl, G., Bierkens, M. F. P., Chambel, A., Cudennec, C., Destouni, G., Fiori, A.,  
632 Kirchner, J. W., McDonnell, J. J., Savenije, H. H. G., Sivapalan, M., Stumpp, C.,  
633 Toth, E., Volpi, E., Carr, G., Lupton, C., Salinas, J., Széles, B., Viglione, A.,  
634 Aksoy, H., Allen, S. T., Amin, A., Andréassian, V., Arheimer, B., Aryal, S. K.,  
635 Baker, V., Bardsley, E., Barendrecht, M. H., Bartosova, A., Batelaan, O.,  
636 Berghuijs, W. R., Beven, K., Blume, T., Bogaard, T., Borges De Amorim, P.,  
637 Böttcher, M. E., Boulet, G., Breinl, K., Brilly, M., Brocca, L., Buytaert, W.,  
638 Castellarin, A., Castelletti, A., Chen, X., Chen, Y., Chen, Y., Chiffard, P., Claps,  
639 P., Clark, M. P., Collins, A. L., Croke, B., Dathe, A., David, P. C., De Barros, F.  
640 P. J., De Rooij, G., Di Baldassarre, G., Driscoll, J. M., Duethmann, D., Dwivedi,  
641 R., Eris, E., Farmer, W. H., Feiccabrino, J., Ferguson, G., Ferrari, E., Ferraris, S.,  
642 Fersch, B., Finger, D., Foglia, L., Fowler, K., Gartsman, B., Gascoin, S., Gaume,  
643 E., Gelfan, A., Geris, J., Gharari, S., Gleeson, T., Glendell, M., Gonzalez  
644 Bevacqua, A., González-Dugo, M. P., Grimaldi, S., Gupta, A. B., Guse, B., Han,  
645 D., Hannah, D., Harpold, A., Haun, S., Heal, K., Helfricht, K., Hermegger, M.,  
646 Hipsey, M., Hlaváčiková, H., Hohmann, C., Holko, L., Hopkinson, C.,  
647 Hrachowitz, M., Illangasekare, T. H., Inam, A., Innocente, C., Istanbuluoglu, E.,  
648 Jarihani, B., et al.: Twenty-three unsolved problems in hydrology (UPH) – a  
649 community perspective, *Hydrology. Sci. J.*, 64, 1141–1158,  
650 <https://doi.org/10.1080/02626667.2019.1620507>, 2019.
- 651 Bolibar, J., Rabatel, A., Gouttevin, I., Zekollari, H., and Galiez, C.: Nonlinear  
652 sensitivity of glacier mass balance to future climate change unveiled by deep  
653 learning, *Nat. Commun.*, 13, 409, <https://doi.org/10.1038/s41467-022-28033-0>,  
654 2022.
- 655 Brovkin, V., Brook, E., Williams, J. W., Bathiany, S., Lenton, T. M., Barton, M.,  
656 DeConto, R. M., Donges, J. F., Ganopolski, A., McManus, J., Praetorius, S., De  
657 Vernal, A., Abe-Ouchi, A., Cheng, H., Claussen, M., Crucifix, M., Gallopín, G.,  
658 Iglesias, V., Kaufman, D. S., Kleinen, T., Lambert, F., Van Der Leeuw, S., Liddy,  
659 H., Loutre, M.-F., McGee, D., Rehfeld, K., Rhodes, R., Seddon, A. W. R., Trauth,  
660 M. H., Vanderveken, L., and Yu, Z.: Past abrupt changes, tipping points and  
661 cascading impacts in the Earth system, *Nat. Geosci.*, 14, 550–558,



- 662 <https://doi.org/10.1038/s41561-021-00790-5>, 2021.
- 663 Chadburn, S. E., Burke, E. J., Cox, P. M., Friedlingstein, P., Hugelius, G., and  
664 Westermann, S.: An observation-based constraint on permafrost loss as a  
665 function of global warming, *Nature Clim. Change*, 7, 340–344,  
666 <https://doi.org/10.1038/nclimate3262>, 2017.
- 667 Chang, Z., Qi, P., Zhang, G., Sun, Y., Tang, X., Jiang, M., Sun, J., and Li, Z.:  
668 Latitudinal characteristics of frozen soil degradation and their response to  
669 climate change in a high-latitude water tower, *CATENA*, 214, 106272,  
670 <https://doi.org/10.1016/j.catena.2022.106272>, 2022.
- 671 Chen, R.-S., Lu, S.-H., Kang, E.-S., Ji, X., Zhang, Z., Yang, Y., and Qing, W.: A  
672 distributed water-heat coupled model for mountainous watershed of an inland  
673 river basin of Northwest China (I) model structure and equations, *Environ. Geol.*,  
674 53, 1299–1309, <https://doi.org/10.1007/s00254-007-0738-2>, 2008.
- 675 Chen, Z., Zhu, R., Yin, Z., Feng, Q., Yang, L., Wang, L., Lu, R., and Fang, C.:  
676 Hydrological response to future climate change in a mountainous watershed in  
677 the Northeast of Tibetan Plateau, *Journal of Hydrology: Regional Studies*, 44,  
678 101256, <https://doi.org/10.1016/j.ejrh.2022.101256>, 2022.
- 679 Connon, R. F., Chasmer, L., Haughton, E., Helbig, M., Hopkinson, C., Sonnentag, O.,  
680 and Quinton, W. L.: The implications of permafrost thaw and land cover change  
681 on snow water equivalent accumulation, melt and runoff in discontinuous  
682 permafrost peatlands, *Hydrol. Process.*, 35, e14363,  
683 <https://doi.org/10.1002/hyp.14363>, 2021.
- 684 Cooper, M. G., Zhou, T., Bennett, K. E., Bolton, W. R., Coon, E. T., Fleming, S. W.,  
685 Rowland, J. C., and Schwenk, J.: Detecting Permafrost Active Layer Thickness  
686 Change From Nonlinear Baseflow Recession, *Water Resour. Res.*, 59,  
687 <https://doi.org/10.1029/2022WR033154>, 2023.
- 688 Cullen, N. J., Sirguey, P., Mölg, T., Kaser, G., Winkler, M., and Fitzsimons, S. J.: A  
689 century of ice retreat on Kilimanjaro: the mapping reloaded, *The Cryosphere*, 7,  
690 419–431, <https://doi.org/10.5194/tc-7-419-2013>, 2013.
- 691 Ding, Y., Zhang, S., Zhao, L., Li, Z., and Kang, S.: Global warming weakening the  
692 inherent stability of glaciers and permafrost, *Sci. Bull.*, 64, 245–253,



- 693 <https://doi.org/10.1016/j.scib.2018.12.028>, 2019.
- 694 Ding, Y., Zhang, S., and Chen, R.: Cryospheric Hydrology: Decode the Largest  
695 Freshwater Reservoir on Earth, *Bulletin of the Chinese Academy of Sciences*, 35,  
696 414–424, 2020.
- 697 Elshamy, M. E., Princz, D., Sapriza-Azuri, G., Abdelhamed, M. S., Pietroniro, A.,  
698 Wheeler, H. S., and Razavi, S.: On the configuration and initialization of a large-  
699 scale hydrological land surface model to represent permafrost, *Hydrol. Earth*  
700 *Syst. Sci.*, 24, 349–379, <https://doi.org/10.5194/hess-24-349-2020>, 2020.
- 701 Farinotti, D., Huss, M., Fürst, J. J., Landmann, J., Machguth, H., Maussion, F., and  
702 Pandit, A.: A consensus estimate for the ice thickness distribution of all glaciers  
703 on Earth, *Nat. Geosci.*, 12, 168–173, <https://doi.org/10.1038/s41561-019-0300-3>,  
704 2019.
- 705 Fenicia, F. and McDonnell, J. J.: Modeling streamflow variability at the regional  
706 scale: (1) perceptual model development through signature analysis, *J. Hydrol.*,  
707 605, 127287, <https://doi.org/10.1016/j.jhydrol.2021.127287>, 2022.
- 708 Gao, H., Wang, J., Yang, Y., Pan, X., Ding, Y., and Duan, Z.: Permafrost Hydrology of  
709 the Qinghai-Tibet Plateau: A Review of Processes and Modeling, *FRONT*  
710 *EARTH SCI*, 8, <https://doi.org/10.3389/feart.2020.576838>, 2021.
- 711 Gao, H., Han, C., Chen, R., Feng, Z., Wang, K., Fenicia, F., and Savenije, H.: Frozen  
712 soil hydrological modeling for a mountainous catchment northeast of the  
713 Qinghai–Tibet Plateau, *Hydrol. Earth Syst. Sci.*, 26, 4187–4208,  
714 <https://doi.org/10.5194/hess-26-4187-2022>, 2022.
- 715 Gao, T., Kang, S., Chen, R., Zhang, T., Zhang, T., Han, C., Tripathee, L., Sillanpää,  
716 M., and Zhang, Y.: Riverine dissolved organic carbon and its optical properties in  
717 a permafrost region of the Upper Heihe River basin in the Northern Tibetan  
718 Plateau, *Sci. Total Environ.*, 686, 370–381,  
719 <https://doi.org/10.1016/j.scitotenv.2019.05.478>, 2019.
- 720 Gilg, O., Kovacs, K. M., Aars, J., Fort, J., Gauthier, G., Grémillet, D., Ims, R. A.,  
721 Meltote, H., Moreau, J., Post, E., Schmidt, N. M., Yannic, G., and Bollache, L.:  
722 Climate change and the ecology and evolution of Arctic vertebrates, *Ann. Ny.*  
723 *Acad. Sci.*, 1249, 166–190, <https://doi.org/10.1111/j.1749-6632.2011.06412.x>,



- 724 2012.
- 725 Han, L. and Menzel, L.: Hydrological variability in southern Siberia and the role of  
726 permafrost degradation, *J. Hydrol.*, 604, 127203,  
727 <https://doi.org/10.1016/j.jhydrol.2021.127203>, 2022.
- 728 Han, P., Long, D., Zhao, F., and Slater, L. J.: Response of Two Glaciers in Different  
729 Climate Settings of the Tibetan Plateau to Climate Change Through Year 2100  
730 Using a Hybrid Modeling Approach, *Water Resour. Res.*, 59,  
731 <https://doi.org/10.1029/2022WR033618>, 2023.
- 732 He, Q., Kuang, X., Chen, J., Hao, Y., Feng, Y., Wu, P., and Zheng, C.: Glacier retreat  
733 and its impact on groundwater system evolution in the Yarlung Zangbo source  
734 region, Tibetan Plateau, *J. Hydrol.: Regional Studies*, 47, 101368,  
735 <https://doi.org/10.1016/j.ejrh.2023.101368>, 2023.
- 736 He, Z., Duethmann, D., and Tian, F.: A meta-analysis based review of quantifying the  
737 contributions of runoff components to streamflow in glacierized basins. *J.*  
738 *Hydrol.*, 603, 126890, <https://doi.org/10.1016/j.jhydrol.2021.126890>, 2021.
- 739 Hu, G., Li, X., Yang, X., Shi, F., Sun, H., and Cui, B.: Identifying Spatiotemporal  
740 Patterns of Hillslope Subsurface Flow in an Alpine Critical Zone on the  
741 Qinghai - Tibetan Plateau Based on Three - Year, High - Resolution Field  
742 Observations, *Water Resour. Res.*, 58, e2022WR032098,  
743 <https://doi.org/10.1029/2022WR032098>, 2022.
- 744 Huss, M. and Fischer, M.: Sensitivity of Very Small Glaciers in the Swiss Alps to  
745 Future Climate Change, *Front. Earth Sci.*, 4,  
746 <https://doi.org/10.3389/feart.2016.00034>, 2016.
- 747 Huss, M. and Hock, R.: Global-scale hydrological response to future glacier mass  
748 loss, *Nature Clim Change*, 8, 135–140, [https://doi.org/10.1038/s41558-017-](https://doi.org/10.1038/s41558-017-0049-x)  
749 [0049-x](https://doi.org/10.1038/s41558-017-0049-x), 2018.
- 750 Huss, M., Jouvett, G., Farinotti, D., and Bauder, A.: Future high-mountain hydrology:  
751 a new parameterization of glacier retreat, *Hydrol. Earth Syst. Sci.*, 14, 815–829,  
752 <https://doi.org/10.5194/hess-14-815-2010>, 2010.
- 753 Intergovernmental Panel On Climate Change (Ipcc): The Ocean and Cryosphere in a  
754 Changing Climate: Special Report of the Intergovernmental Panel on Climate



- 755 Change, 1st ed., Cambridge University Press,  
756 <https://doi.org/10.1017/9781009157964>, 2022.
- 757 Jiang, R., Li, T., Liu, D., Fu, Q., Hou, R., Li, Q., Cui, S., and Li, M.: Soil infiltration  
758 characteristics and pore distribution under freezing–thawing conditions, *The*  
759 *Cryosphere*, 15, 2133–2146, <https://doi.org/10.5194/tc-15-2133-2021>, 2021.
- 760 Jones, M. W., Sebestyen, S. D., Dymond, S. F., Ng, G. H. C., and Feng, X.: Soil frost  
761 controls streamflow generation processes in headwater catchments, *J. Hydrol.*,  
762 617, <https://doi.org/10.1016/j.jhydrol.2022.128801>, 2023.
- 763 Kaplan Pastiriková, L., Hrbáček, F., Uxa, T., and Láska, K.: Permafrost table  
764 temperature and active layer thickness variability on James Ross Island,  
765 Antarctic Peninsula, in 2004–2021, *Sci. Total Environ.*, 869, 161690,  
766 <https://doi.org/10.1016/j.scitotenv.2023.161690>, 2023.
- 767 Li, L., Xu, Z., Zuo, D., and Zhao, J.: A grid-based integrated surface–groundwater  
768 model (GISMOD), *J. Water Clim. Change*, 7, 296–320,  
769 <https://doi.org/10.2166/wcc.2015.006>, 2016.
- 770 Li, X., Jin, H., Sun, L., Wang, H., Huang, Y., He, R., Chang, X., Yu, S., and Zang, S.:  
771 TTOP - model - based maps of permafrost distribution in Northeast China for  
772 1961 - 2020, *Permafrost periglac.*, 33, 425–435,  
773 <https://doi.org/10.1002/ppp.2157>, 2022.
- 774 Liu, Z., Cuo, L., and Sun, N.: Tracking snowmelt during hydrological surface  
775 processes using a distributed hydrological model in a mesoscale basin on the  
776 Tibetan Plateau, *J. Hydrol.*, 616, <https://doi.org/10.1016/j.jhydrol.2022.128796>,  
777 2023.
- 778 McCarthy, M., Meier, F., Fatichi, S., Stocker, B. D., Shaw, T. E., Miles, E.,  
779 Dussaillant, I., and Pellicciotti, F.: Glacier Contributions to River Discharge  
780 During the Current Chilean Megadrought, *Earth’s Future*, 10, e2022EF002852,  
781 <https://doi.org/10.1029/2022EF002852>, 2022.
- 782 Michel, A., Schaefli, B., Wever, N., Zekollari, H., Lehning, M., and Huwald, H.:  
783 Future water temperature of rivers in Switzerland under climate change  
784 investigated with physics-based models, *Hydrol. Earth Syst. Sci.*, 26, 1063–1087,  
785 <https://doi.org/10.5194/hess-26-1063-2022>, 2022.



- 786 Miner, K., Turetsky, M., Malina, E., Bartsch, A., Tamminen, J., McGuire, A., Fix, A.,  
787 Sweeney, C., Elder, C., and Miller, C.: Permafrost carbon emissions in a  
788 changing Arctic, *Nature Reviews Earth & Environmental*, 3, 55–67,  
789 <https://doi.org/10.1038/s43017-021-00230-3>, 2022.
- 790 Mohammed, A. A., Cey, E. E., Hayashi, M., and Callaghan, M., V.: Simulating  
791 preferential flow and snowmelt partitioning in seasonally frozen hillslopes,  
792 *Hydrol. Process.*, 35, <https://doi.org/10.1002/hyp.14277>, 2021.
- 793 Moreno, P. I., Fercovic, E. I., Soteres, R. L., Ugalde, P. I., Sagredo, E. A., and Villa-  
794 Martínez, R. P.: Glacier and terrestrial ecosystem evolution in the Chilotan  
795 archipelago sector of northwestern Patagonia since the Last Glacial Termination,  
796 *Earth-Science Reviews*, 235, 104240,  
797 <https://doi.org/10.1016/j.earscirev.2022.104240>, 2022.
- 798 Negi, V. S., Tiwari, D. C., Singh, L., Thakur, S., and Bhatt, I. D.: Review and  
799 synthesis of climate change studies in the Himalayan region, *Environ Dev*  
800 *Sustain*, 24, 10471–10502, <https://doi.org/10.1007/s10668-021-01880-5>, 2022.
- 801 Nury, A. H., Sharma, A., Mehrotra, R., Marshall, L., and Cordery, I.: Projected  
802 Changes in the Tibetan Plateau Snowpack Resulting From Rising Global  
803 Temperatures, *J. Geophys. Res.-Atmos.*, 127,  
804 <https://doi.org/10.1029/2021JD036201>, 2022.
- 805 Pomeroy, J. W., Brown, T., Fang, X., Shook, K. R., Pradhananga, D., Armstrong, R.,  
806 Harder, P., Marsh, C., Costa, D., Krogh, S. A., Aubry-Wake, C., Annand, H.,  
807 Lawford, P., He, Z., Kompanizare, M., and Lopez Moreno, J. I.: The cold regions  
808 hydrological modelling platform for hydrological diagnosis and prediction based  
809 on process understanding, *J. Hydrol.*, 615, 128711,  
810 <https://doi.org/10.1016/j.jhydrol.2022.128711>, 2022.
- 811 Pothula, S. K. and Adams, B. J.: Community assembly in the wake of glacial retreat:  
812 A meta - analysis, *Glob. Chang Biol*, 28, 6973–6991,  
813 <https://doi.org/10.1111/gcb.16427>, 2022.
- 814 Qin, D., Yao, T., Ding, Y., and Ren, J.: Classification and Geographical Distribution of  
815 Cryosphere, in: *Introduction to Cryospheric Science*. Springer Singapore,  
816 Singapore, 33–79, [https://doi.org/10.1007/978-981-16-6425-0\\_2](https://doi.org/10.1007/978-981-16-6425-0_2), 2021.



- 817 Rabatel, A., Ceballos, J. L., Micheletti, N., Jordan, E., Braitmeier, M., González, J.,  
818 Mölg, N., Ménégoz, M., Huggel, C., and Zemp, M.: Toward an imminent  
819 extinction of Colombian glaciers?, *Geografiska Annaler: Series A, Phys Geog*,  
820 100, 75–95, <https://doi.org/10.1080/04353676.2017.1383015>, 2018.
- 821 Ragetli, S., Immerzeel, W. W., and Pellicciotti, F.: Contrasting climate change impact  
822 on river flows from high-altitude catchments in the Himalayan and Andes  
823 Mountains, *Proc. Natl. Acad. Sci. U.S.A.*, 113, 9222–9227,  
824 <https://doi.org/10.1073/pnas.1606526113>, 2016.
- 825 Rasul, G., Pasakhala, B., Mishra, A., and Pant, S.: Adaptation to mountain cryosphere  
826 change: issues and challenges, *Clim Dev*, 12, 297–309,  
827 <https://doi.org/10.1080/17565529.2019.1617099>, 2020.
- 828 Rosier, S. H. R., Reese, R., Donges, J. F., De Rydt, J., Gudmundsson, G. H., and  
829 Winkelmann, R.: The tipping points and early warning indicators for Pine Island  
830 Glacier, West Antarctica, *The Cryosphere*, 15, 1501–1516,  
831 <https://doi.org/10.5194/tc-15-1501-2021>, 2021.
- 832 Stecher, G., Hohensinner, S., and Herrnegger, M.: Changes in the water retention of  
833 mountainous landscapes since the 1820s in the Austrian Alps, *Front. Environ.*  
834 *Sci.*, 11, 1219030, <https://doi.org/10.3389/fenvs.2023.1219030>, 2023.
- 835 Sun, B., Liu, J., Ren, F., Li, H., Zhang, G., Ma, J., Ma, B., and Li, Z.: Effects of  
836 seasonal freeze–thaw and wind erosion on runoff and sediment yields of three  
837 loamy slopes of Loess Plateau, China, *CATENA*, 215, 106309,  
838 <https://doi.org/10.1016/j.catena.2022.106309>, 2022.
- 839 Tang, G., Clark, M. P., Knoben, W. J. M., Liu, H., Gharari, S., Arnal, L., Beck, H. E.,  
840 Wood, A. W., Newman, A. J., and Papalexiou, S. M.: The Impact of  
841 Meteorological Forcing Uncertainty on Hydrological Modeling: A Global  
842 Analysis of Cryosphere Basins, *Water Resour. Res.*, 59, e2022WR033767,  
843 <https://doi.org/10.1029/2022WR033767>, 2023.
- 844 Teng, J., Liu, J., Zhang, S., and Sheng, D.: Frost heave in coarse-grained soils:  
845 experimental evidence and numerical modelling, *GEOTECHNIQUE*, 73, 1100–  
846 1111, <https://doi.org/10.1680/jgeot.21.00182>, 2022.
- 847 Teutschbein, C. and Seibert, J.: Bias correction of regional climate model simulations





- 848 for hydrological climate-change impact studies: Review and evaluation of  
849 different methods, *J. Hydrol.*, 456–457, 12–29,  
850 <https://doi.org/10.1016/j.jhydrol.2012.05.052>, 2012.
- 851 Van Der Geest, K. and Van Den Berg, R.: Slow-onset events: a review of the evidence  
852 from the IPCC Special Reports on Land, Oceans and Cryosphere, *CURR OPIN*  
853 *ENV SUST*, 50, 109–120, <https://doi.org/10.1016/j.cosust.2021.03.008>, 2021.
- 854 Vincent, C. and Thibert, E.: Brief communication: Non-linear sensitivity of glacier  
855 mass balance to climate attested by temperature-index models, *The Cryosphere*,  
856 17, 1989–1995, <https://doi.org/10.5194/tc-17-1989-2023>, 2023.
- 857 Wang, J., Chen, X., Gao, M., Hu, Q., and Liu, J.: Changes in nonlinearity and stability  
858 of streamflow recession characteristics under climate warming in a large  
859 glaciated basin of the Tibetan Plateau, *Hydrol. Earth Syst. Sci.*, 26, 3901–3920,  
860 <https://doi.org/10.5194/hess-26-3901-2022>, 2022a.
- 861 Wang, K., Zhang, T., and Clow, G. D.: Permafrost Thermal Responses to  
862 Asymmetrical Climate Changes: An Integrated Perspective, *Geophys. Res. Lett.*,  
863 50, e2022GL100327, <https://doi.org/10.1029/2022GL100327>, 2023.
- 864 Wang, Q., Qi, J., Wu, H., Zeng, Y., Shui, W., Zeng, J., and Zhang, X.: Freeze-Thaw  
865 cycle representation alters response of watershed hydrology to future climate  
866 change, *CATENA*, 195, <https://doi.org/10.1016/j.catena.2020.104767>, 2020.
- 867 Wang, S., Yang, Y., and Che, Y.: Global Snow- and Ice-Related Disaster Risk: A  
868 Review, *Nat. Hazards Rev.*, 23, 03122002,  
869 [https://doi.org/10.1061/\(ASCE\)NH.1527-6996.0000584](https://doi.org/10.1061/(ASCE)NH.1527-6996.0000584), 2022b.
- 870 Wang, X., Chen, R., Liu, G., Yang, Y., Song, Y., Liu, J., Liu, Z., Han, C., Liu, X., Guo,  
871 S., Wang, L., and Zheng, Q.: Spatial distributions and temporal variations of the  
872 near-surface soil freeze state across China under climate change, *Global*  
873 *Planetary Change*, 172, 150–158,  
874 <https://doi.org/10.1016/j.gloplacha.2018.09.016>, 2019.
- 875 Wang, Y., Yang, H., Gao, B., Wang, T., Qin, Y., and Yang, D.: Frozen ground  
876 degradation may reduce future runoff in the headwaters of an inland river on the  
877 northeastern Tibetan Plateau, *J. Hydrol.*, 564, 1153–1164,  
878 <https://doi.org/10.1016/j.jhydrol.2018.07.078>, 2018.



- 879 Wei, L., Zhao, W., Feng, X., Han, C., Li, T., Qi, J., and Li, Y.: Freeze-thaw  
880 desertification of alpine meadow in Qilian Mountains and the implications for  
881 alpine ecosystem management, *CATENA*, 232, 107471,  
882 <https://doi.org/10.1016/j.catena.2023.107471>, 2023.
- 883 Wen, Y., Liu, B., Jiang, H., Li, T.-Y., Zhang, B., and Wu, W.: Initial soil moisture  
884 prewinter affects the freeze–thaw profile dynamics of a Mollisol in Northeast  
885 China, *CATENA*, 234, 107648, <https://doi.org/10.1016/j.catena.2023.107648>,  
886 2024.
- 887 Whitfield, P. H., Kraaijenbrink, P. D. A., Shook, K. R., and Pomeroy, J. W.: The  
888 spatial extent of hydrological and landscape changes across the mountains and  
889 prairies of Canada in the Mackenzie and Nelson River basins based on data from  
890 a warm-season time window, *Hydrol. Earth Syst. Sci.*, 25, 2513–2541,  
891 <https://doi.org/10.5194/hess-25-2513-2021>, 2021.
- 892 Wiersma, P., Aerts, J., Zekollari, H., Hrachowitz, M., Drost, N., Huss, M.,  
893 Sutanudjaja, E. H., and Hut, R.: Coupling a global glacier model to a global  
894 hydrological model prevents underestimation of glacier runoff, *Hydrol. Earth  
895 Syst. Sci.*, 26, 5971–5986, <https://doi.org/10.5194/hess-26-5971-2022>, 2022.
- 896 Wilby, R. L. and Harris, I.: A framework for assessing uncertainties in climate change  
897 impacts: Low - flow scenarios for the River Thames, UK, *Water Resour. Res.*, 42,  
898 2005WR004065, <https://doi.org/10.1029/2005WR004065>, 2006.
- 899 Xu, C., Li, Z., Wang, F., Ha, L., Yagoub, Y. E., and Jin, S.: Recent geodetic mass  
900 balance and extent changes of very small glaciers in the Hulugou Basin, Central  
901 Qilian Mountains, China, *J Earth Syst Sci.*, 128, 47,  
902 <https://doi.org/10.1007/s12040-019-1067-z>, 2019.
- 903 Yang, M., Li, Z., Anjum, M. N., Kayastha, R., Kayastha, R. B., Rai, M., Zhang, X.,  
904 and Xu, C.: Projection of Streamflow Changes Under CMIP6 Scenarios in the  
905 Urumqi River Head Watershed, Tianshan Mountain, China, *Front. Earth Sci.*, 10,  
906 857854, <https://doi.org/10.3389/feart.2022.857854>, 2022.
- 907 Yao, T., Bolch, T., Chen, D., Gao, J., Immerzeel, W., Piao, S., Su, F., Thompson, L.,  
908 Wada, Y., Wang, L., Wang, T., Wu, G., Xu, B., Yang, W., Zhang, G., Zhao, P.,  
909 2022. The imbalance of the Asian water tower. *NATURE REVIEWS EARTH &*



- 910 ENVIRONMENT 3, 618–632. <https://doi.org/10.1038/s43017-022-00299-4>
- 911 Yao, Y., Zheng, C., Andrews, C. B., Scanlon, B. R., Kuang, X., Zeng, Z., Jeong, S.-J.,  
912 Lancia, M., Wu, Y., and Li, G.: Role of Groundwater in Sustaining Northern  
913 Himalayan Rivers, *Geophys. Res. Lett.*, 48,  
914 <https://doi.org/10.1029/2020GL092354>, 2021.
- 915 Zekollari, H., Huss, M., Farinotti, D., and Lhermitte, S.: Ice - Dynamical Glacier  
916 Evolution Modeling—A Review, *Reviews of Geophysics*, 60, e2021RG000754,  
917 <https://doi.org/10.1029/2021RG000754>, 2022.
- 918 Zhang, S., Gao, X., Zhang, X., and Hagemann, S.: Projection of glacier runoff in  
919 Yarkant River basin and Beida River basin, Western China, *Hydrol. Process.*, 26,  
920 2773–2781, <https://doi.org/10.1002/hyp.8373>, 2012.
- 921 Zhang, T., Li, D., and Lu, X.: Response of runoff components to climate change in the  
922 source-region of the Yellow River on the Tibetan plateau, *Hydrol. Process.*, 36,  
923 <https://doi.org/10.1002/hyp.14633>, 2022.
- 924 Zhang, Z., Wang, Y., Ma, Z., and Lv, M.: Response mechanism of soil structural  
925 heterogeneity in permafrost active layer to freeze-thaw action and vegetation  
926 degradation, *CATENA*, 230, <https://doi.org/10.1016/j.catena.2023.107250>, 2023.